SCIENCE CHINA
Information Sciences

• RESEARCH PAPER •

November 2021, Vol. 64 212202:1–212202:16
https://doi.org/10.1007/s11432-020-3107-7

Distributed multilane merging for connected autonomous vehicle platooning

Jingkai WU[1], Yafei WANG[1], Zhaokun SHEN[2], Lin WANG[2], Haiping DU[3] & Chengliang YIN[1*]

[1]*School of Mechanical Engineering, Shanghai Jiao Tong University, Shanghai* 200240*, China;*
[2]*School of Electrical and Electronics Engineering, Shanghai Jiao Tong University, Shanghai* 200240*, China;*
[3]*School of Electrical, Computer and Telecommunications Engineering, University of Wollongong, Wollongong* 2522*, Australia*

Received 4 May 2020/Revised 8 July 2020/Accepted 1 October 2020/Published online 20 October 2021

Abstract In the context of coordination of connected autonomous vehicles (CAVs), the platooning operation is a promising application. The formulation of a single stream of CAVs is conducive to traffic efficiency and merging operations extend the benefits for multilane road users. However, the problem of simultaneous merging and platooning lacks comprehensive investigation. A solution is formulated in this paper through a new scheme that considers inter-vehicle safety distance constraints and distributed deployment utilizing local inter-vehicle information exchanges. A distributed consensus-based controller synthesized with a collision avoidance design is developed to direct the CAVs to maintain the velocity and spacing required to avoid inter-vehicle collisions. Furthermore, a framework fusing an agent motion model with vehicle controllers based on a dynamics model that facilitates both longitudinal and lateral controls is proposed, contributing to a cross-model planning-tracking controller. Theoretical proof of asymptotic stability of the proposed controller and its collision avoidance capability are also elaborated. The merging and platooning function was tested in a hardware-in-the-loop (HiL) experiment, demonstrating the precise tracking performance and comparable merging responses to a typical multiagent system. In comparison with trajectory-based merging algorithms, the proposed framework is able to achieve finer stepwise tracking results without centralized coordination or predefined trajectories.

Keywords platoon, merging, connected autonomous vehicle, multiagent system, distributed controller

Citation Wu J K, Wang Y F, Shen Z K, et al. Distributed multilane merging for connected autonomous vehicle platooning. Sci China Inf Sci, 2021, 64(11): 212202, https://doi.org/10.1007/s11432-020-3107-7

1 Introduction

Connected autonomous vehicles (CAVs) serve as the information and actuation nodes of an intelligent transportation system (ITS). Equipped with autonomous and communication technologies, a group of CAVs are expected to complete coordinated tasks automatically with safety guarantees and traffic efficiency [1]. The use of shared information to coordinate these vehicles challenges traditional vehicle control by extending the problem of a single vehicle to multiple ones, raising concerns about communication and coordination mechanisms. Hence, various preliminary scenarios, such as nonsignalized intersection control [2], ramp merging [3,4], and lane changing [5,6], have been investigated so that researchers can focus on specific application requirements.

Platooning [7] is a typical application scenario for CAVs that requires coordinated vehicle maneuvers. To assemble a line of vehicles, the key issues of constructing the information flow topology, node dynamics, distributed controller, and formation geometry [8] need to be resolved. The existing literature reveals that spacing control realized through vehicle longitudinal control has received most of the attention, whereas the lateral control is often omitted. The same-lane location setting is reasonable as the sole consideration of platooning. Situations where CAVs are initially dispersed in different lanes are cases where current platooning methods may not apply. Some initial demonstrations have shown great potential

* Corresponding author (email: clyin1965@sjtu.edu.cn)

in expanding current platooning applications to more complicated cases. Refs. [9, 10] utilized designed protocols to conduct the merging of two platoons in separate lanes. Ref. [11] also considered the merging of two platoons but placed more emphasis on the spacing policy so that steering can be carried out as long as the spacing is appropriate. Ref. [12] utilized a centralized trajectory-based approach to realize the merging of CAVs into a platoon but lacked vehicle models to implement actual steering commands. In these studies, the lateral vehicle controllers are not explicitly formulated and spacing adjustments need to be accomplished before the merging happens, which could result in time-consuming cascading spacing adjustments. Therefore, to better utilize the lane resources, a more practical merging and platooning scheme that handles both steering and throttling simultaneously needs to be put forward.

The important merging phase in assembling a platoon from multiple lanes requires lane-changing operations. Existing studies that focus on trajectory generation [13], merging traffic [14], and trajectory prediction [15] are mostly related to an isolated controlled vehicle. In multivehicle cases, they may add an extra communication and computation burden to notify other vehicles of the planned trajectories, and the subsequent conflict resolution mechanism [16] may not be suitable for multivehicle implementations. In reality, vehicle-to-vehicle (V2V) technology can reliably support 10 Hz basic safety messages (BSMs) or cooperative awareness messages (CAMs) communication among vehicles with critical information transfer, such as real-time vehicle positions and velocities [17]. Multi-CAV interactions demand the simultaneous fulfillment of the required control performance and real-time requirements with limited communication cost, which is a necessary but challenging task.

Widely adopted in multiagent systems, consensus control is based on coordinating controllable agents to move and reach a desired common state [18]. Such control is generally conducted by autonomous agents with information exchanges with nearby agents. This locally lightweight feature suits the requirements of the merging and platooning task [19]. Taking advantage of the consensus control's inherent consistency with the platooning requirement, we propose to apply this coordination idea combined with vehicle dynamics considerations through newly-designed controllers to realistic vehicle models.

In this paper, we aim to solve the problem of multilane merging and platooning. Practical considerations of maintenance of a safe distance, information exchanges, and lane usages are considered through a distributed consensus controller design. A framework named planning and tracking with feedforward steering (PaTFS) is proposed to assemble both coordinated agent motion and vehicle-based trajectory tracking controls. This combination of models, which ensures feasible vehicle inputs through the combined controller structure, is further strengthened through a conversion scheme of acceleration input into vehicle-compatible steering commands. Hardware-in-the-loop (HiL) experiments were conducted to verify the real-time implementation of the proposed framework as well as to demonstrate its precise tracking performance compared with other predefined trajectory-based methods.

The contributions of this paper are as follows.

(1) To improve the traffic efficiency through a better vehicle platooning scheme, a PaTFS framework is proposed to accomplish the multilane merging and platooning task. It provides a solution by integrating the simplified motion model in the platooning operation and the actual vehicle handling that relies on vehicle dynamics. This design provides vehicle-compatible coordinated steering and longitudinal control to facilitate simultaneous merging and platooning with real-time performance and better lane usage.

(2) To formulate the necessary inputs and reference states for PaTFS, a distributed controller is proposed for the specific sequential platooning scenario supported by a theoretically-guaranteed safe and reachable platooning configuration design. A sequential platooning configuration is proven to ensure a safe distance while avoiding the possible local minima caused by collision avoidance potential fields. Additionally, the asymptotic stability of the proposed controller in the presence of nonlinear collision avoidance terms is proven.

(3) The framework bears precise control performance at each timestep, which was verified through a HiL experiment in comparison with fixed merging trajectory methods. The idea of cross-model stepwise planning and tracking control is realized with effective reference tracking performance. The successful conveyance of motion information to the vehicle actuator inputs in the framework is expected to be compatible with other motion models and vehicle controllers to accommodate different coordination tasks for future studies.

The rest of the paper is organized as follows: Section 2 describes the problem of multilane merging and platoon formation and introduces the tracking dynamics model. Section 3 proposes a consensus-based controller for a second-order point model with a collision avoidance mechanism and demonstrates its association process with vehicle dynamics. Section 4 carries out the stability analysis and the proof

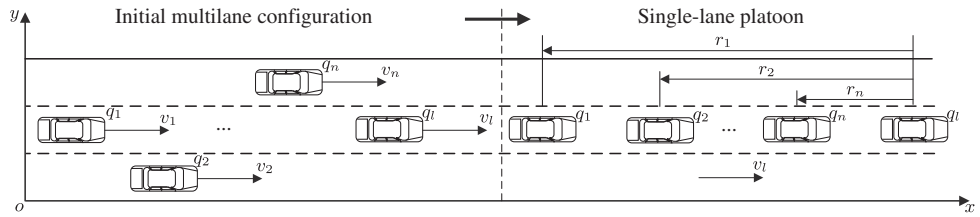

Figure 1 Illustration of the scenario. The following CAVs $1, 2, \ldots, n$ initially located in multiple lanes are expected to achieve a single-lane platoon formation with a desired distance $\boldsymbol{r}_i$ relative to the leader and maintain the same velocity $\boldsymbol{v}_l$ as the leader.

of collision avoidance guarantee of the proposed scheme. Section 5 verifies the proposed planning and control scheme through HiL experiments in multilane merging and platooning scenarios. A comparison of other different models and schemes is carried out. Section 6 gives the conclusion and prospective future research topics.

2 Problem formulation and model description

This paper considers a homogeneous platoon composed of n identical sequentially ordered CAVs following a leader vehicle. Initially dispersed in different lanes, the following CAVs exhibit velocity and spacing differences. The objective is to eliminate such inconsistencies during the process of platoon formation and make the CAVs follow a stable line configuration.

2.1 Problem formulation

Among the n following CAVs, CAV $i, i = 1, \ldots, n$ is characterized by the following double integrator model:

$$\begin{cases} \dot{\boldsymbol{q}}_i(t) = \boldsymbol{v}_i(t), \\ \dot{\boldsymbol{v}}_i(t) = \boldsymbol{u}_i(t), \end{cases} \tag{1}$$

where $\boldsymbol{q}_i(t) = [x_i(t), y_i(t)]^{\mathrm{T}}$ and $\boldsymbol{v}_i(t) = [v_i^x(t), v_i^y(t)]^{\mathrm{T}} \in \mathbb{R}^2$ are the position and velocity, respectively. The leader vehicle l has the same model with $\boldsymbol{q}_l(t) = [x_l(t), y_l(t)]^{\mathrm{T}}$ and $\boldsymbol{v}_i = [v_l^x(t), v_l^y(t)]^{\mathrm{T}}$. The desired following position of CAV i is characterized as $\boldsymbol{q}_i^*(t)$, and the desired relative position of CAV i to the leader can be characterized by $\boldsymbol{r}_i = \boldsymbol{q}_i^*(t) - \boldsymbol{q}_l(t) = [r_i^x, r_i^y]^{\mathrm{T}}$, which is set as a constant vector here.

Without loss of generality, we set up a straight road aligned with the positive x axis, and the leader vehicle is driving in the positive x direction. Thus, the following definition concludes the requirements for the multilane merging and platooning problem.

Definition 1. In a straight road with a positive x driving direction, a leader bears constant velocity $\boldsymbol{v}_l = [v_l^x(t), 0]^{\mathrm{T}}, v_l^x(t) > 0$ without steering, $\boldsymbol{y}_l(t) \equiv y_l(0)$. The desired single-lane platoon formation of CAV i is then characterized by $\boldsymbol{r}_i = [r_i^x, 0]^{\mathrm{T}}$ and $r_1^x < \cdots < r_i^x < \cdots < r_n^x$.

The multilane platoon formation control objective is then formulated. Design a control method $\boldsymbol{u}_i$ so that the following CAVs $i, i = 1, \ldots, n$ in multilane locations can ultimately achieve a platoon formation in the same lane as the leader l. Moreover, a predefined vehicle spacing vector $\boldsymbol{r}_i$ needs to be reached.

$$\lim_{t\to\infty}(\boldsymbol{q}_i(t) - \boldsymbol{q}_l(t) - \boldsymbol{r}_i) = 0, \quad \lim_{t\to\infty}(\boldsymbol{v}_i(t) - \boldsymbol{v}_l(t)) = 0. \tag{2}$$

An illustration of the scenario is given in Figure 1. In the following Sections 3–5, t in the time-dependent variables will be omitted for concise expression if no extra declaration is given.

Remark 1. The model in (1) characterizes the moving states of the following CAVs but is not viewed as the vehicle plant. Its integration in the PaTFS framework for reference generation and feedforward control of the CAVs will be detailed in Section 3.

2.2 Dynamics model description

Note that the basic motion states and vehicle interaction can be defined through the simplified motion model described in Subsection 2.1; however, the actual vehicle states and inputs are not fully characterized by it. An actual vehicle dynamics model is still required to derive vehicle control input to each of the CAVs.

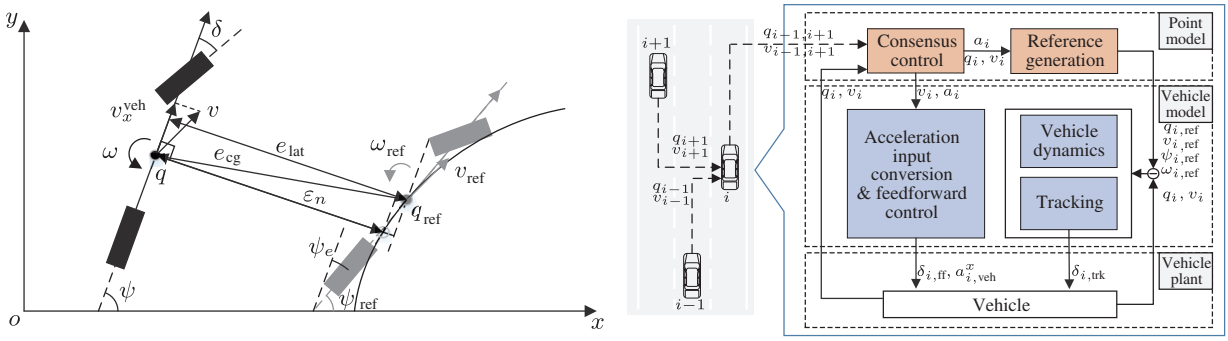

(a) (b)

Figure 2 (Color online) (a) The tracking models. The gray vehicle represents the reference. (b) The block diagram of the proposed PaTFS framework for the merging and platoon formation task.

The lateral reference tracking model is introduced to facilitate the necessary lateral control. Figure 2(a) shows a typical tracking model, where $\boldsymbol{e}_{\rm cg} = [x, y]^{\rm T} - [x_{\rm ref}, y_{\rm ref}]^{\rm T} = [e_x, e_y]^{\rm T}$ is the deviation from the vehicle's center of gravity to the desired tracking position. The deviation from the desired yaw angle $\psi_{\rm ref}$ to the vehicle's actual yaw angle ψ is characterized by $\psi_e = \psi - \psi_{\rm ref}$. The yaw rates of the actual vehicle and the reference model are denoted by ω and $\omega_{\rm ref}$, respectively. How these reference and error states are acquired will be discussed in Section 3. According to [20], a small ψ_e facilitates the following approximation: $e_{\rm lat} \approx \varepsilon_n$, and a tracking model to minimize $e_{\rm lat}$ can be formulated as

$$\begin{bmatrix} \dot{\varepsilon}_n \\ \ddot{\varepsilon}_n \\ \dot{\psi}_e \\ \ddot{\psi}_e \end{bmatrix} = \begin{bmatrix} 0 & 1 & 0 & 0 \\ 0 & \frac{-M_1}{v^x_{\rm veh}} & M_1 & \frac{-M_2}{v^x_{\rm veh}} \\ 0 & 0 & 0 & 1 \\ 0 & \frac{-I_1}{v^x_{\rm veh}} & I_1 & \frac{-I_2}{v^x_{\rm veh}} \end{bmatrix} \begin{bmatrix} \varepsilon_n \\ \dot{\varepsilon}_n \\ \psi_e \\ \dot{\psi}_e \end{bmatrix} + \begin{bmatrix} 0 \\ \frac{C_f}{m} \\ 0 \\ \frac{l_f c_f}{I_z} \end{bmatrix} \delta - \begin{bmatrix} 0 \\ \frac{M_2 + (v^x_{\rm veh})^2}{v^x_{\rm veh}} \\ 0 \\ \frac{I_2}{v^x_{\rm veh}} \end{bmatrix} \omega_{\rm ref}, \tag{3}$$

where $M_1 = (C_f + C_r)/m, M_2 = (l_f C_f - l_r C_r)/m$; l_f and l_r are the distances from the center of gravity to the center of the front and rear axles, respectively; m is the vehicle mass; $I_1 = (l_f C_f - l_r C_r)/I_z, I_2 = (l_f^2 C_f + l_r^2 C_r)/I_z$; I_z is the yaw moment of inertia; $v^x_{\rm veh}$ is the longitudinal velocity; $l = l_f + l_r$ is the wheel base; C_f and C_r are the known front and rear tire cornering stiffness, respectively; δ is the front wheel steering control input.

So far, the developed point motion model and vehicle dynamics-based tracking model are still separate modules. A joint framework that integrates them is detailed in Section 3.

3 PaTFS framework design

This section introduces the PaTFS framework that handles the problem formulated in Subsection 2.1. The platooning objective is achieved using a consensus-based controller applicable for the second-order point motion model. As this model merely generates an acceleration input that cannot be directly applied to actual CAVs, multiple modules were designed to formulate the integrated PaTFS framework, which accomplishes the necessary reference trajectory generation, control input conversion, and tracking control.

The diagram of the proposed framework illustrated in Figure 2(b) describes the system integration. Within this framework, the consensus-based controller generates the basic motions needed for the coordination of the CAVs. The generated reference states are then fed to the tracking and feedforward controller to generate feasible vehicle actuator inputs. Each module design is explained in the following Subsections 3.1–3.3.

3.1 Consensus-based controller design

Viewing a graph $\mathcal{G}$ composed of CAVs as vertices $\mathcal{V} = \{1, 2, \ldots, n\}$ and the connections between them as edges $\mathcal{E} = \{(ij) \in \mathcal{V} \times \mathcal{V}\}$, we can use the adjacency matrix $A = [a_{ij}]$ containing the nonnegative components a_{ij} to characterize whether a pair of CAVs i and j share the information: $a_{ij} > 0$, means that the CAV i can receive the information of CAV j, and $a_{ij} = 0$, means that it cannot.

A controller that takes into account the information shared through the communication topology is proposed as follows:

$$\begin{aligned}\boldsymbol{u}_i = &-\sum_{j=1}^{n}\alpha a_{ij}[(\boldsymbol{q}_i-\boldsymbol{q}_j-\boldsymbol{r}_i+\boldsymbol{r}_j)+\gamma(\boldsymbol{v}_i-\boldsymbol{v}_j)]-\epsilon k_i[(\boldsymbol{q}_i-\boldsymbol{q}_l-\boldsymbol{r}_i)+\gamma(\boldsymbol{v}_i-\boldsymbol{v}_l)]\\ &-\sum_{j=1}^{n}\phi_C(\|x_i-x_j\|)\boldsymbol{t}_{ij}-\phi_L(\mathrm{sign}(y_i(0)-y_l(0))(y_i-y_l)+w)\boldsymbol{t}_{L,i},\end{aligned}\tag{4}$$

where $\alpha\in\mathbb{R}$ is a positive gain parameter and $k_i\in\mathbb{R}$ is a nonnegative number denoting the extent to which CAV i is influenced by the leader. The parameter $\gamma=\mathrm{diag}(\gamma_x,\gamma_y)\in\mathbb{R}^2$ is a weighted positive definite gain matrix with $\gamma_x,\gamma_y>0$.

The two terms ϕ_C and ϕ_L are introduced as repulsive forces that effectively prevent collisions among the agents [21] and ensure lane-keeping. $\boldsymbol{t}_{ij}=[t_{ij}^x,t_{ij}^y]^{\mathrm{T}}=([x_j-x_i,0]^{\mathrm{T}})/\|x_j-x_i\|$ is a unit vector pointing from i to j in the x direction, and $\boldsymbol{t}_{L,i}$ will be explained later.

The collision-avoidance force generated by a potential function is given as follows:

$$\phi_C(\|x_{ij}\|)=\begin{cases}\rho_h(\|x_{ij}\|/r_{\mathrm{act}})\phi_d(\|x_{ij}\|), & i\neq j,\\ 0, & i=j,\end{cases}\tag{5}$$

where

$$\phi_d(s)=\frac{1}{(s-d)^2},\ s>d,\quad \rho_h(z)=\begin{cases}1, & z\in[0,h),\\ \dfrac{1}{2}[1+\cos(\pi\frac{z-h}{1-h})], & z\in[h,1],\\ 0, & \text{otherwise},\end{cases}\tag{6}$$

$\|x_{ij}\|=\|x_i-x_j\|$ represents the longitudinal distance between vehicles i and j. In addition, r_{act} is the effective radius of the potential field, which is slightly smaller than the desired spacing $\|r_i-r_j\|$; d is the smallest distance allowed between the CAVs. $h\in[0,1]$ is an adjustable term. The function $\phi(\|x_{ij}\|)$ serves as a basic action function, and $\rho_h(\|x_{ij}\|/r_{\mathrm{act}})$ is a bump function from [22] that helps smooth this action function.

The potential field is effective when $\|x_{ij}\|\in(d,r_{\mathrm{act}}]$. Note that as $\|x_{ij}\|\to d^+$, the repulsive force may grow infinitely, $\phi_C(\|x_{ij}\|)\to\infty$. In reality, this case may never occur, and it is proven in the bounded Lyapunov analysis in Section 4 with collision avoidance guarantee.

To better describe the formulation of the lane-keeping force, we introduce the error states:

$$\tilde{\boldsymbol{q}}_i=\boldsymbol{q}_i-\boldsymbol{q}_l-\boldsymbol{r}_i,\quad \tilde{\boldsymbol{v}}_i=\boldsymbol{v}_i-\boldsymbol{v}_l.\tag{7}$$

Thus,

$$x_i-x_l-r_i^x=\tilde{x}_i,\quad y_i-y_l-r_i^y=y_i-y_l=\tilde{y}_i.\tag{8}$$

The lane-keeping force ϕ_L is formulated similar to that of ϕ_C:

$$\phi_L(\mathrm{sign}(\tilde{y}_i(0))\tilde{y}_i+w)=\rho_h((\mathrm{sign}(\tilde{y}_i(0))\tilde{y}_i+w)/w)\phi_0((\mathrm{sign}(\tilde{y}_i(0))\tilde{y}_i+w)),\tag{9}$$

where w is half of the lane width and the sign function indicates whether the CAV i is merging into the desired lane from the right or from the left. $\boldsymbol{t}_{L,i}=[0,-\mathrm{sign}(\tilde{y}(0))]^{\mathrm{T}}$ is a unit vector pointing from the initial lane to the desired lane.

Remark 2. Compared with the existing studies on platooning [19,23], the distributed controller in (4) employs practical distance and lane keeping functions, which is a realistic concern. The lateral control input will also be handled in the PaTFS framework for practical steering inputs generation.

3.2 Reference generation and tracking

The difference between the point and vehicle models makes the direct application of (4) infeasible; thus, a local controller is necessary. Knowing that the point model provides only position and velocity information, we treat (4) as a reference generator. The states of the point model $q_{\mathrm{ref}},v_{\mathrm{ref}}$ can then serve as the reference states of a planned trajectory.

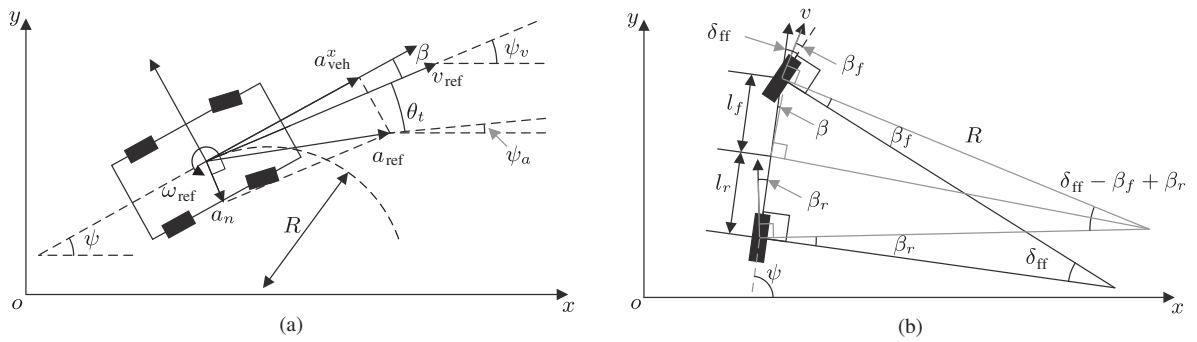

Figure 3 (a) The relationship between acceleration and velocity. The vectors a_{ref} and v_{ref} generated by the point model are used to deduce the sideslip angle β and turning radius R. (b) The geometric relationships of the sideslip angles: β_f, β_r, β and the feedforward steering angle δ_{ff} that needs to be derived.

The error states are acquired through:

$$\begin{aligned}
&\varepsilon_n = -(e_x)\sin(\psi) + (e_y)\cos(\psi),\\
&\psi_e = \psi - \psi_{\text{ref}},\\
&\dot{\varepsilon}_n = -e_x\cos(\psi)\omega - e_y\sin(\psi)\omega - \dot{e}_x\sin(\psi) + \dot{e}_y\cos(\psi),\\
&\dot{\psi}_e = \omega - \omega_{\text{ref}}.
\end{aligned} \tag{10}$$

Note that most of the parameters are available except the desired heading ψ_{ref} and the yaw rate ω_{ref} information, which need to be derived as they are not inherited in the point motion model. Therefore, we propose a conversion scheme for this purpose. From Figure 3(a), the acceleration normal to the velocity is

$$a_n = a_{\text{ref}}\sin(\theta_t) = v^2_{\text{ref}}/R = \omega^2_{\text{ref}}R, \tag{11}$$

where $\theta_t = \psi_a - \psi_v$ is the included angle between the acceleration and velocity and R is the turning radius. The desired yaw rate ω_{ref} is therefore achieved by

$$\omega_{\text{ref}} = \frac{a_{\text{ref}}}{v_{\text{ref}}}\sin(\theta_t), \tag{12}$$

where the reference acceleration a_{ref} and velocity v_{ref} are taken from the motion model in (1). The calculation of the desired heading ψ_{ref} is given in Subsection 3.3. Because all reference states and error states can be calculated and applied to the lateral tracking model (3), the steering angle δ_{trk} can be achieved through a linear quaratic regulator (LQR) tracking controller from [20]:

$$\delta_{\text{trk}} = -K_{\text{LQR}}\begin{bmatrix}\boldsymbol{e}_{\text{cg}} & \dot{\boldsymbol{e}}_{\text{cg}} & \psi_e & \dot{\psi}_e\end{bmatrix}^{\text{T}}, \tag{13}$$

where K_{LQR} is the optimal gain.

3.3 Acceleration input conversion

A fast feedforward calculation is introduced here, mapping the acceleration to actual vehicle control inputs. In particular, the steering angle δ_{ff} and longitudinal acceleration a^x_{veh} are derived.

The turning radius is already derived in (11). The assumption of the steady cornering state then yields the geometric relationship shown in Figure 3(b), by which the sideslip angle can be derived using [24]:

$$\beta_f = \frac{mv^2l_r}{2lC_fR}, \quad \beta_r = \frac{mv^2l_f}{2lC_rR}, \tag{14}$$

where R is the turning radius.

Information on the geometric relationships of the sideslip and steering angles is also acquired as follows:

$$R = \frac{l}{\delta_{\text{ff}} - \beta_f + \beta_r}. \tag{15}$$

From (11), (14) and (15), the steering angle is acquired as follows:

$$\delta_{\mathrm{ff}} = \frac{a_{\mathrm{ref}} \sin(\theta_t)}{v^2} \left(l + \frac{mv^2 l_r}{2lC_f} - \frac{mv^2 l_f}{2lC_r} \right), \tag{16}$$

where the subscript ff represents the feedforward control.

The vehicle heading attainable as the angular relationships in Figures 3(a) and (b) indicates:

$$\beta + \beta_r = \frac{l_r}{R}, \quad \psi = \psi_v + \beta. \tag{17}$$

Thus, the longitudinal acceleration is expressed as

$$a^x_{\mathrm{veh}} = a_{\mathrm{ref}} \cos(\psi_a - \psi) = a_{\mathrm{ref}} \cos \left[\psi_a - \psi_v - \frac{a \sin(\theta_t)}{v^2} \left(l_r - \frac{mv^2 l_f}{2lC_r} \right) \right]. \tag{18}$$

With (13) and (16) combined, the steering control is expressed as

$$\delta = \delta_{\mathrm{ff}} + \delta_{\mathrm{trk}}. \tag{19}$$

Recall that the reference heading ψ_{ref} is needed in Subsection 3.2, which can be derived in the same way as in (17):

$$\psi_{\mathrm{ref}} = \frac{a_{\mathrm{ref}} \sin(\theta_t)}{v^2_{\mathrm{ref}}} \left(l_r - \frac{mv^2 l_f}{2lC_r} \right). \tag{20}$$

4 Stability analysis

This section provides the theoretical analysis of the distributed controller (4) with provable stability and safety guarantee.

The distributed controller's inherent network topology design has been found to greatly influence the stability of CAVs in the platooning process [8]. Some assumptions regarding its properties are listed.

Assumption 1. The graph $\mathcal{G}$ is connected and undirected.

Assumption 2. At least one vehicle has access to the leader information: $\exists i, k_i > 0$.

Then, the following conditions hold: $A = [a_{ij}]$ is symmetric, and $\mathcal{G}$'s Laplacian matrix L and pinning matrix $K = \mathrm{diag}(k_1, \ldots, k_i, \ldots, k_n)$ are positive semidefinite.

Lemma 1 ([25])**.** Given Assumptions 1 and 2, the summation $L + K$ is positive definite.

Intuitively, a direct extension of Lemma 1 is the following.

Corollary 1. Given the same condition in Lemma 1 on L and K, $M = \alpha L + \epsilon K$ is nonsingular for $\alpha, \epsilon \in \mathbb{R}, \alpha, \epsilon > 0$.

To demonstrate the stability of the proposed controller, the error states are formulated along with the corresponding input representation.

Substituting the corresponding terms in (4) with (7) we have

$$\begin{cases} \dot{\tilde{\boldsymbol{q}}}_i = \dot{\boldsymbol{q}}_i - \dot{\boldsymbol{q}}_l = \tilde{\boldsymbol{v}}_i, \\ \dot{\tilde{\boldsymbol{v}}}_i = \dot{\boldsymbol{v}}_i - \dot{\boldsymbol{v}}_l = \dot{\boldsymbol{v}}_i = \boldsymbol{u}_i, \end{cases} \tag{21}$$

and the input $\boldsymbol{u}_i$ has the following dynamics:

$$\begin{aligned} \boldsymbol{u}_i = &- \sum_{j=1}^{n} \alpha a_{ij} [(\tilde{\boldsymbol{q}}_i - \tilde{\boldsymbol{q}}_j) + \gamma(\tilde{\boldsymbol{v}}_i - \tilde{\boldsymbol{v}}_j)] - \epsilon k_i (\tilde{\boldsymbol{q}}_i + \gamma \tilde{\boldsymbol{v}}_i) \\ &- \sum_{j=1}^{n} \phi_C(\|\tilde{x}_i - \tilde{x}_j + r^x_i - r^x_j\|) \boldsymbol{t}_{ij} - \phi_L(\mathrm{sign}(\tilde{y}_i(0)) \tilde{y}_i + w) \boldsymbol{t}_{L,i}. \end{aligned} \tag{22}$$

Writing (22) in a compact form using $M = \alpha L + \epsilon K$:

$$\boldsymbol{u}_i = - \sum_{j=1}^{n} m_{ij} \tilde{\boldsymbol{q}}_j - \gamma \sum_{j=1}^{n} m_{ij} \tilde{\boldsymbol{v}}_j - \sum_{j=1}^{n} \phi_C(\|\tilde{\boldsymbol{q}}_i - \tilde{\boldsymbol{q}}_j + \boldsymbol{r}_i - \boldsymbol{r}_j\|) \boldsymbol{t}_{ij} - \phi_L(\mathrm{sign}(\tilde{y}_i(0)) \tilde{y}_i + w) \boldsymbol{t}_{L,i}. \tag{23}$$

where $M = [m_{ij}]$.

Theorem 1. The control scheme (4) leads the following vehicles from different lanes to merge into one lane to form a platoon:

(1) with a uniform velocity: $\boldsymbol{v}_i = \boldsymbol{v}_j, \forall i, j, i \neq j$,

(2) without causing any collision: $\|\boldsymbol{q}_{ij}\| - d > 0$,

if $\tilde{\boldsymbol{q}}(0)$ and $\tilde{\boldsymbol{v}}(0)$ are bounded and $\|x_{ij}(0)\| > d$.

Proof. We start by proving the first statement of Theorem 1. Constructing the following Lyapunov function:

$$V = \frac{1}{2}\tilde{\boldsymbol{v}}^{\mathrm{T}}\tilde{\boldsymbol{v}} + \frac{1}{2}\tilde{\boldsymbol{q}}^{\mathrm{T}}(M \otimes I_2)^{\mathrm{T}}\tilde{\boldsymbol{q}} + \frac{1}{2}\sum_{i=1}^{n}\sum_{j=1}^{n}\int_{\|\tilde{x}_i - \tilde{x}_j + r_i^x - r_j^x\|}^{r_{\mathrm{act}}} \phi_C(s)\mathrm{d}s + \sum_{i=1}^{n}\int_{\mathrm{sign}(\tilde{y}_i(0))\tilde{y}_i + w}^{w} \phi_L(s)\mathrm{d}s, \quad (24)$$

where I_2 is an identity matrix of size 2 and $\otimes$ denotes the Kronecker product. The state variables are defined as $\tilde{\boldsymbol{v}} = [\tilde{\boldsymbol{v}}_1^{\mathrm{T}}, \ldots, \tilde{\boldsymbol{v}}_n^{\mathrm{T}}]^{\mathrm{T}}$ and $\tilde{\boldsymbol{q}} = [\tilde{\boldsymbol{q}}_1^{\mathrm{T}}, \ldots, \tilde{\boldsymbol{q}}_n^{\mathrm{T}}]^{\mathrm{T}}$. It is easy to verify that $V \geqslant 0$. Take the derivative of (24):

$$\begin{aligned}\dot{V} = &\sum_{i=1}^{n}\tilde{\boldsymbol{v}}_i^{\mathrm{T}}\left(-\sum_{j=1}^{n}m_{ij}\tilde{\boldsymbol{q}}_j - \gamma\sum_{j=1}^{n}m_{ij}\tilde{\boldsymbol{v}}_j\right) + \sum_{i=1}^{n}\tilde{\boldsymbol{v}}_i^{\mathrm{T}}\sum_{j=1}^{n}m_{ij}\tilde{\boldsymbol{q}}_j \\ &- \sum_{i=1}^{n}\tilde{\boldsymbol{v}}_i^{\mathrm{T}}\sum_{j=1}^{n}\phi_C(\|\tilde{x}_i - \tilde{x}_j + r_i^x - r_j^x\|)\boldsymbol{t}_{ij} - \sum_{i=1}^{n}\tilde{\boldsymbol{v}}_i^{\mathrm{T}}\phi_L(\mathrm{sign}(\tilde{y}_i(0))\tilde{y}_i + w)\boldsymbol{t}_{L,i} \\ &+ \frac{1}{2}\sum_{i=1}^{n}\sum_{j=1}^{n}(\tilde{v}_i^x - \tilde{v}_j^x)\phi_C(\|\tilde{x}_i - \tilde{x}_j + r_i^x - r_j^x\|)t_{ij}^x - \sum_{i=1}^{n}\tilde{v}_i^y\phi_L(\mathrm{sign}(\tilde{y}_i(0))\tilde{y}_i + w)\mathrm{sign}(\tilde{y}_i(0)). \quad (25)\end{aligned}$$

The following condition holds given the symmetry of the forces ϕ_C:

$$-\sum_{i=1}^{n}\tilde{\boldsymbol{v}}_i^{\mathrm{T}}\sum_{j=1}^{n}\phi_C(\|\tilde{x}_i - \tilde{x}_j + r_i - r_j\|)\boldsymbol{t}_{ij} + \frac{1}{2}\sum_{i=1}^{n}\sum_{j=1}^{n}(\tilde{v}_i^x - \tilde{v}_j^x)\phi_C(\|\tilde{x}_i - \tilde{x}_j + r_i^x - r_j^x\|)t_{ij}^x = 0. \quad (26)$$

Similar symmetry analysis can be obtained because the unit vector $\boldsymbol{t}_{L,i}$ is perpendicular to the x direction:

$$-\sum_{i=1}^{n}\tilde{\boldsymbol{v}}_i^{\mathrm{T}}\phi_L(\mathrm{sign}(\tilde{y}_i(0))\tilde{y}_i + w)\boldsymbol{t}_{L,i} - \sum_{i=1}^{n}\tilde{v}_i^y\phi_L(\mathrm{sign}(\tilde{y}_i(0))\tilde{y}_i + w)\mathrm{sign}(\tilde{y}_i(0)) = 0. \quad (27)$$

Eqs. (25)–(27) together indicate:

$$\dot{V} = \tilde{\boldsymbol{v}}^{\mathrm{T}}(M \otimes \gamma)^{\mathrm{T}}\tilde{\boldsymbol{v}} \leqslant 0. \quad (28)$$

Note that M, according to Corollary 1, and γ are positive definite. The term $M \otimes \gamma$ is thus positive definite and $\dot{V} = 0$ only when $\tilde{\boldsymbol{v}} = 0$, which implies that velocity consensus is achieved.

To prove the second statement of Theorem 1, recall that $\tilde{\boldsymbol{q}}(0)$ and $\tilde{\boldsymbol{v}}(0)$ are bounded and $\|\boldsymbol{q}_i(0) - \boldsymbol{q}_j(0)\| > \|x_{ij}(0)\| > d$. This indicates that the initial situation $V(0)$ is bounded. Similar to the idea of [26], suppose a collision is happening between CAVs i and j at time t_c, $\phi_C(\|x_{ij}(t_c)\|) \to \infty$ as $\|x_i - x_j\| - d \to 0$, meaning that $V(t_c) > V(0)$, which contradicts $\dot{V} \leqslant 0$ in (25). This proves that $\|\boldsymbol{q}_i - \boldsymbol{q}_j\| > \|x_{ij}\| > d$ holds.

Corollary 2. If the following CAVs are initially sequentially located in different lanes: $x_1(0) < \cdots < x_i(0) < \cdots < x_n(0)$, then $x_1(t) < \cdots < x_i(t) < \cdots < x_n(t)$ always holds.

The proof follows similar approaches as those used for proving the second statement of Theorem 1 and is omitted here.

Remark 3. $\tilde{\boldsymbol{q}}(0)$ and $\tilde{\boldsymbol{v}}(0)$ are bounded and $\|x_{ij}(0)\| > d$. These settings on the initial states result from the obvious physical limitations of the CAV velocities and inter-vehicle distances. Hence, the nonexistence of any collisions at the very beginning makes platooning possible.

Remark 4. Velocity consensus does not directly imply that the desired following positions are reached. To ensure $\tilde{\boldsymbol{q}}_i = 0$, further analysis is needed.

To ensure that convergence to the desired platoon configuration is achievable, some practical settings suitable for the vehicle and traffic characteristics were elaborated with the following assumption.

Assumption 3. The sequential platoon is assumed to hold the following conditions:

(1) The desired spacing is equal: $\|\boldsymbol{r}_i - \boldsymbol{r}_{i+1}\| = \|\boldsymbol{r}\| > r_{\text{act}}, i = 1, \ldots, n-1$ and $d < r_{\text{act}} < 2d$.

(2) Only CAV n, which is the nearest to the leader l, has access to the information of l: $k_1, \ldots, k_{n-1} = 0, k_n > 0$, and the following CAVs have an undirected nearest-neighbor communication topology:

$$m_{ij} = \begin{cases} -\alpha a_{ij}, & \|i-j\| = 1, i = 2, \ldots, n-1, \\ 0, & \|i-j\| \geqslant 2, \\ \alpha a_{1,2}, & i = j = 1, \\ \alpha(a_{i,i+1} + a_{i,i-1}), & i = j, i = 2, \ldots, n-1, \\ \alpha a_{i,i-1} + \epsilon k_n, & i = j = n. \end{cases} \tag{29}$$

Assumption 3 constrains the problem to a scenario where the following CAVs with their nearest-neighbor communication topology are expected to form a straight-lane constant-spacing sequential platoon with the leader l at a constant velocity, which is a typical setting [27].

The following theorem is then subsequently constructed to prove the convergence of the position errors.

Theorem 2. If velocity consensus $\tilde{v} = 0$ is reached, the following conditions hold:

(1) No collision avoidance forces exist, which means $\phi_C(\|\tilde{x}_i - \tilde{x}_j + r_i - r_j\|) = 0, \forall i, j, i \neq j$;

(2) No lane-keeping forces exist, which is $\phi_L(\text{sign}(\tilde{y}_i(0))\tilde{y}_i + w) = 0, \forall i$;

(3) The desired position of each CAV is reached: $\tilde{\boldsymbol{q}} = 0$.

Proof. We start the proof with the first statement of Theorem 2. The velocity consensus, $\tilde{\boldsymbol{v}} = 0$ as well as $\dot{\tilde{\boldsymbol{v}}} = 0$, simplifies (23) to the following form:

$$\begin{aligned} \sum_{i=1}^{n} \tilde{\boldsymbol{q}}_i^{\mathrm{T}} \dot{\tilde{\boldsymbol{v}}}_i = \sum_{i=1}^{n} \tilde{\boldsymbol{q}}_i^{\mathrm{T}} \left(-\sum_{j=1}^{n} m_{ij} \tilde{\boldsymbol{q}}_j \right) - \sum_{i=1}^{n} \sum_{j=1}^{n} \tilde{\boldsymbol{q}}_i^{\mathrm{T}} \phi_C(\|\tilde{x}_i - \tilde{x}_j + r_i^x - r_j^x\|) \boldsymbol{t}_{ij} \\ - \sum_{i=1}^{n} \tilde{\boldsymbol{q}}_i^{\mathrm{T}} \phi_L(\text{sign}(\tilde{y}_i(0))\tilde{y}_i + w) \boldsymbol{t}_{L,i} = 0. \end{aligned} \tag{30}$$

From Corollary 2 and the second statement of Theorem 1, $\|x_i - x_{i\pm h}\| > hd, h \geqslant 1, i = 2, \ldots, n-1, i + h \in [1, i-1] \cup [i+1, n]$. Note that Eq. (6) and the first statement of Assumption 3 indicate that the collision avoidance force is effective only when$\|x_i - x_{i+h}\| < r_{\text{act}} < 2d$, precluding any condition that a collision avoidance force exists when $h \geqslant 2$,

$$\phi_C(\|x_{i,i\pm h}\|) = 0, \quad h \geqslant 2, \ i = 2, \ldots, n-1. \tag{31}$$

Assume there exist two consecutive CAVs $i, i+1, i = 2, \ldots, n-1$ that have repulsive forces generated by the potential fields under the condition where all CAVs reach a velocity consensus $\tilde{\boldsymbol{v}} = 0$, $\dot{\tilde{\boldsymbol{v}}} = 0$. Given (31) and the second statement of Assumption 3, the control of CAV i is

$$\begin{aligned} \boldsymbol{u}_i =& - m_{i,i+1}\tilde{\boldsymbol{q}}_{i+1} - m_{i,i}\tilde{\boldsymbol{q}}_i - m_{i,i-1}\tilde{\boldsymbol{q}}_{i-1} - \phi_C(\|x_{i,i+1}\|)\boldsymbol{t}_{i,i+1} - \phi_C(\|x_{i,i-1}\|)\boldsymbol{t}_{i,i-1} - \phi_L(\tilde{y}_i) \\ =& - \alpha a_{i,i+1}(\tilde{\boldsymbol{q}}_i - \tilde{\boldsymbol{q}}_{i+1}) - \alpha a_{i-1,i}(\tilde{\boldsymbol{q}}_i - \tilde{\boldsymbol{q}}_{i-1}) - \phi_C(\|x_{i,i+1}\|)\boldsymbol{t}_{i,i+1} - \phi_C(\|x_{i,i-1}\|)\boldsymbol{t}_{i,i-1} - \phi_L(\tilde{y}_i) \\ =& \boldsymbol{f}_{i,i+1} + \boldsymbol{f}_{i,i-1} + \phi_{C,i,i+1} + \phi_{C,i,i-1} + \phi_{L,i} = 0 \end{aligned} \tag{32}$$

in which $\boldsymbol{f}_{i,i+1} = -\alpha a_{i,i+1}(\tilde{\boldsymbol{q}}_i - \tilde{\boldsymbol{q}}_{i+1})$, $\boldsymbol{f}_{i,i-1} = -\alpha a_{i-1,i}(\tilde{\boldsymbol{q}}_i - \tilde{\boldsymbol{q}}_{i-1})$, $\phi_{C,i,j} = -\phi_C(\|\tilde{x}_i - \tilde{x}_j + r_i^x - r_j^x\|)\boldsymbol{t}_{i,j}$ and $\phi_{L,i} = -\phi_L(\text{sign}(\tilde{y}_i(0))\tilde{y}_i + w)\boldsymbol{t}_{L,i}$. To continue the proof, we analyze how the CAV i is balanced in the x direction through simplifying (32):

$$f_{i,i+1}^x + f_{i,i-1}^x + \phi_{C,i,i+1}^x + \phi_{C,i,i-1}^x = 0 \tag{33}$$

with the fact that the lane-keeping force $\phi_{L,i}$ has 0 component in its x direction.

Given the first statement of Assumption 3 and Corollary 2, we have

$$\begin{aligned} f_{i,i+1}^x &= -\alpha a_{i,i+1}(x_i - x_{i+1} - r_i^x + r_{i+1}^x) = \alpha a_{i,i+1}(\|\boldsymbol{q}_i - \boldsymbol{q}_{i+1}\| \cos\zeta - \|\boldsymbol{r}\|) \\ &< \alpha a_{i,i+1}(r_{\text{act}} \cos\zeta - \|\boldsymbol{r}\|) \leqslant \alpha a_{i,i+1}(r_{\text{act}} - \|\boldsymbol{r}\|) < 0, \end{aligned} \tag{34}$$

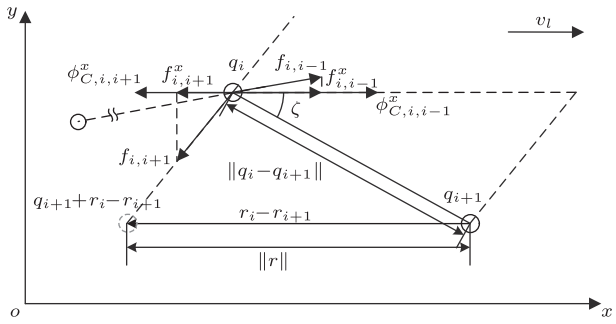

Figure 4 Illustration of the forces exerted on a CAV i when a velocity consensus is reached, with the assumption of a repulsive force.

as $\alpha, a_{i,i+1} > 0$. In addition, the x component of $\phi_C(\boldsymbol{q}_{i,i+1})$: $\phi^x_C(\boldsymbol{q}_{i,i+1}) = \phi_C(\|\tilde{x}_i - \tilde{x}_{i+1} + r^x_i - r^x_{i+1}\|)(x_i - x_{i+1})/\|x_i - x_{i+1}\| < 0$. Then Eq. (33) becomes

$$f^x_{i,i-1} + \phi^x_{C,i,i-1} = -f^x_{i,i+1} - \phi^x_{C,i,i+1} > 0, \tag{35}$$

as Figure 4, containing all forces exerted on CAV i, shows.

A similar analysis could be carried out iteratively for the following CAVs $i-1, \ldots, 2$, and Eq. (35) still holds, which indicates that a CAV i always needs a following CAV $i-1$ to balance itself. However, for the last CAV 1, no following CAV exists, and the x component of input u_1 is

$$u^x_1 = f^x_{1,2} + \phi^x_{C,1,2} < 0, \tag{36}$$

which contradicts (33). Thus, no repulsive forces exist when the velocity consensus is reached: $\phi_C(\|\tilde{x}_i - \tilde{x}_{i+1} + r^x_i - r^x_{i+1}\|) = 0, \forall i, j, i \neq j, \tilde{\boldsymbol{q}}_i = \tilde{\boldsymbol{q}}_j = 0$.

The first statement of Theorem 2 is proven. We can now rewrite (30) in the following form:

$$\sum_{i=1}^{n} \tilde{\boldsymbol{q}}_i^{\mathrm{T}} \dot{\tilde{\boldsymbol{v}}}_i = \sum_{i=1}^{n} \tilde{\boldsymbol{q}}_i^{\mathrm{T}} \left(-\sum_{j=1}^{n} m_{ij} \tilde{\boldsymbol{q}}_j \right) + \sum_{i=1}^{n} -\tilde{\boldsymbol{q}}_i^{\mathrm{T}} \phi_L(\mathrm{sign}(\tilde{y}_i(0))\tilde{y}_i + w)\boldsymbol{t}_{L,i} = 0. \tag{37}$$

From (9), it is easy to verify that

$$-\tilde{\boldsymbol{q}}_i^{\mathrm{T}} \phi_L(\mathrm{sign}(\tilde{y}_i(0))\tilde{y}_i + w)\boldsymbol{t}_{L,i} = \tilde{y}_i \phi_L(\mathrm{sign}(\tilde{y}_i(0))\tilde{y}_i + w)\mathrm{sign}(\tilde{y}_i(0)) \leqslant 0. \tag{38}$$

Eq. (38) along with $\sum_{i=1}^{n} \tilde{\boldsymbol{q}}_i^{\mathrm{T}}(-\sum_{j=1}^{n} m_{ij}\tilde{\boldsymbol{q}}_j) \leqslant 0$ indicates Eq. (37) holds only when $\tilde{\boldsymbol{q}}_i = 0, \forall i$, proving the second and the third statements of Theorem 2.

Remark 5. Ref. [28] indicates that the potential-generated local minima may exist. Theorem 2 proves the nonexistence of potential-generated forces at the equilibrium. This indicates that no local minima caused by the potential fields exists. Thus, the local minima problem is avoided and a global optimum is reached.

Theorem 3. The desired single-lane platoon is formulated through the controller (4) without collisions among the CAVs.

Proof. This can be directly concluded from Theorems 1 and 2.

The coordination protocol of CAVs established in this section yields further issues of implementations, which is discussed in Section 5.

5 HiL experiment and analysis

As described in this section, we construct two sets of scenarios to validate the proposed framework.

5.1 Scenario 1: triplet interaction

The first scenario is a basic case where three following vehicles located in three different lanes need to form a platoon with the desired spacing and distance relative to the leader. This scenario, which consists

Table 1 Parameter settings

Symbol	Description	Value	Unit
$\boldsymbol{q}(0)$	CAVs' initial positions	$[1, 6, 20, 2, 40, 10]^{\mathrm{T}}$	m
$\boldsymbol{v}(0)$	CAVs' initial velocities	$[21, 0, 20, 0, 19, 0]^{\mathrm{T}}$	m/s
$\boldsymbol{q}_l(0)$	Leader's initial position	$[60, 6]^{\mathrm{T}}$	m
$\boldsymbol{v}_l$	Leader's velocity	$[15, 0]^{\mathrm{T}}$	m/s
$\boldsymbol{r}$	Desired displacement from the leader	$[-45, 0, -30, 0, -15, 0]^{\mathrm{T}}$	m
d	Minimum allowed distance	9	m
α, ϵ	Gain parameters	$\alpha = 0.2, \epsilon = 0.24$	–
γ	Gain parameters	$\gamma = \mathrm{diag}(6, 4.8)$	–
k	Pinning matrix	$k = [0, 0, 1]$	–
A	Adjacency matrix	$\begin{bmatrix} 0 & 1 & 0 \\ 1 & 0 & 1 \\ 0 & 1 & 0 \end{bmatrix}$	–
T_s	Communication interval	0.1	s
T	Simulation time	60	s

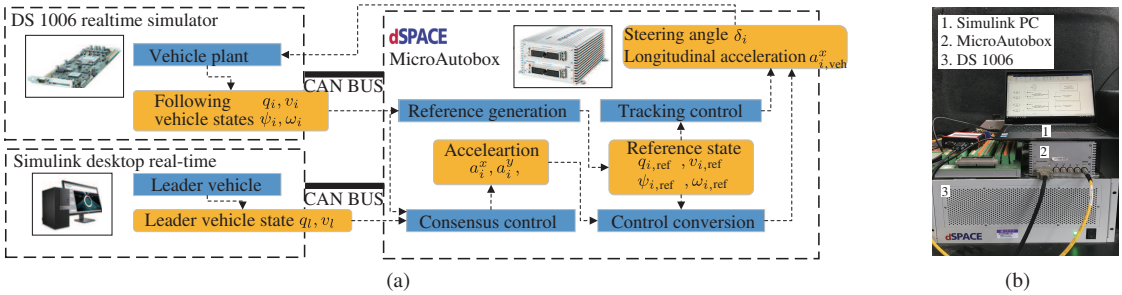

Figure 5 (Color online) (a) illustrates the composition of the HiL experiment platform and the signal flow. Hardware connections and the data transferred within the network are given. (b) shows the actual implemented testbed.

Table 2 Vehicle parameters

Symbol	Description	Value	Unit
m	CAV's mass	1830	kg
I_z	CAV's yaw moment	3234	$\mathrm{kg} \cdot \mathrm{m}^2$
l_f	Distance from the front axle to the CoG	1.45	m
l_r	Distance from the rear axle to the CoG	1.6	m
l	Wheel base	3.05	m
C_f, C_r	Cornering stiffness	98.3	kN/rad

of a triplet of CAVs is a minimum configuration for the multilane interaction activities [11]. In this work, the necessary tests on longitudinal and lateral controls were performed using PaTFS. We demonstrate the validity of the PaTFS framework through comparison with other simplified implementations of the proposed controller: the point model (PT) and the planning-and-tracking without feedforward (PaT) schemes. PT is based on the controller (4) applied only to the point model without vehicle dynamics consideration, which acts as a baseline. PaT is a degraded version of PaTFS that does not consider feedforward steering (16). The effect of lacking this part of the control will be presented and explained later. The initial position and velocity information is listed in Table 1 along with other control parameters. Note that $\boldsymbol{r} = [\boldsymbol{r}_1^{\mathrm{T}}, \ldots, \boldsymbol{r}_n^{\mathrm{T}}]^{\mathrm{T}}$.

The HiL experiment platform described in Figure 5(a) is designed for the high-fidelity verification of vehicle controllers. The platform is composed of a MicroAutobox, a DS 1006 simulator, and a PC running Simulink, which are connected through a controller area network (CAN) bus. The experiment parameters are listed in Table 2. Other parameters include the gain of the LQR tracking controller: $Q = \mathrm{diag}(0.01, 0, 0, 0)$ and $R = 5$.

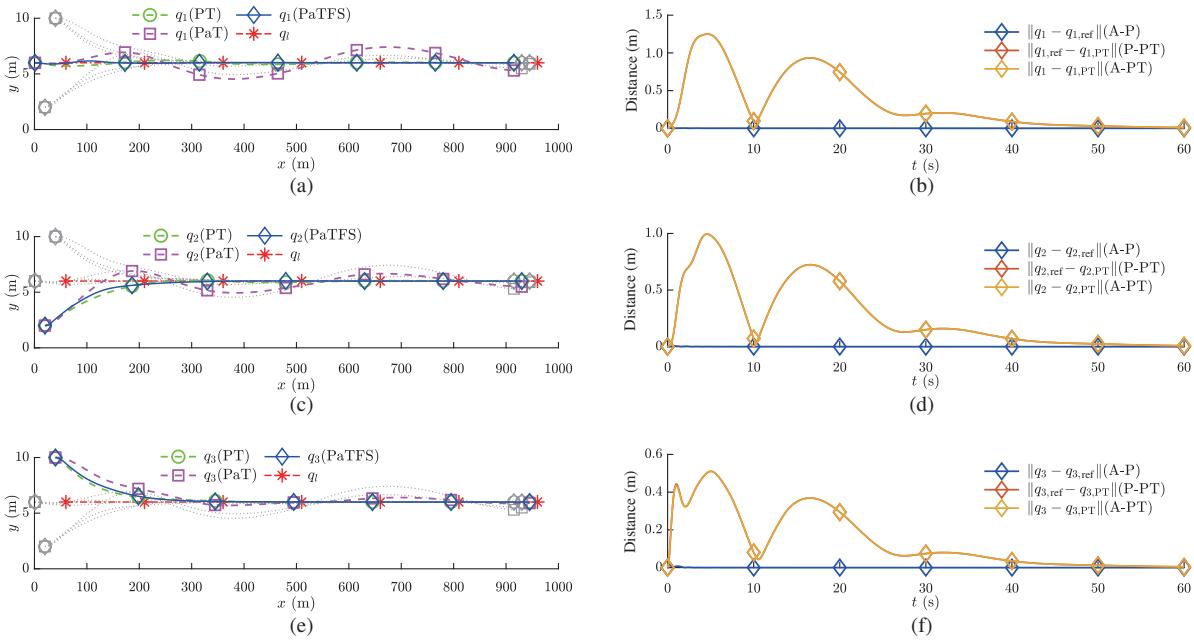

Figure 6 (Color online) (a), (c) and (e) illustrate the trajectories of CAV 1, CAV 2 and CAV 3 during the merging and platooning operations using PT, PaT, and PaTFS respectively. In each subfigure, each of the colored lines denotes the trajectory of a particular CAV with one of the aforementioned three controllers while the gray dotted lines represent the results of other CAVs. The position error state evolutions of CAV 1, CAV 2 and CAV 3 are illustrated in (b), (d) and (f). The differences in CAV positions using PT and PaTFS are given. These values compare the actual (A) and planned (P) positions of the PaTFS with those of the PT. Deviations from PT in the merging phase were ultimately alleviated.

5.1.1 *Comparison of trajectories and error evolutions*

Figure 6 shows the trajectories of each following CAV. In each subfigure, the colored lines indicate the trajectories of the same CAV under the PT, PaT, and PaTFS models. The leader's trajectory is also depicted as the reference. Though multilane merging and platooning was accomplished in all cases, scrutinization on how the trajectories evolve indicates the differences of each controller's performance.

For PaT, although its state responses were comparable to those of PT or PaTFS, it showed the most evident fluctuations in trajectories. The loss of information during the lateral acceleration acquisition led to inaccuracies in the derivation of the steering maneuvers, which impedes the settlement of lateral deviations along the desired lane. PaTFS in contrast, acted in accordance with the PT model, obtaining better convergence performance owing to the more effective steering control. All CAVs with PaTFS showed lower fluctuation magnitudes from the target lane's centerline than those with PaT. In addition, all CAVs with PaTFS navigated to the target lane before CAV 1 reached 200 m; at that point, CAVs with PaT showed larger deviations.

Compared with the point model movements, PaTFS showed similar convergence performance, which is desirable in forming the platoon in less time and lower lane occupation. The concern that differences in the motion patterns of PaTFS and PT may compromise the platooning performance is addressed in the following discussion.

The following analysis is based on the trajectories produced by the PaTFS framework only. The actual position, the reference position, and the point model position of CAV i are denoted by $\boldsymbol{q}_i$, $\boldsymbol{q}_{i,\mathrm{ref}}$, and $\mathrm{q}_{i,\mathrm{PT}}$, respectively. The errors between them depicted in Figure 6 reveal the tracking performance of the proposed method. The process through which the step-wise planning and tracking scheme is able to achieve the same equilibrium as under the PT model can be observed. The following error analysis is given.

- In P-PT, all CAV planned trajectories gradually converge to the PT results. The relatively large deviations observed in the initial stages are caused by the steering maneuvers and spacing adjustments, which are attenuated after the velocity changing stage is complete.
- In A-P, the vanishing tracking errors between the actual and planned reference positions reveal the high precision of stepwise reference-following behaviors.
- In A-PT, the convergence of the actual and PT state differences can be observed when inter-vehicle

Table 3 RMS and final values of the tracking errors for 3 states of the following CAVs using the PaTFS framework

	Case	CAV 1	CAV 2	CAV 3
RMS (m)	A-P	4.0544×10^{-4}	6.6270×10^{-4}	1.5333×10^{-3}
	P-PT	0.4982	0.3906	0.2076
	A-PT	0.4981	0.3906	0.2074
Final error (m)	A-P	2.5362×10^{-7}	1.9859×10^{-7}	1.0090×10^{-7}
	P-PT	9.9724×10^{-3}	7.8153×10^{-3}	3.9435×10^{-3}
	A-PT	9.9723×10^{-3}	7.8152×10^{-3}	3.9434×10^{-3}

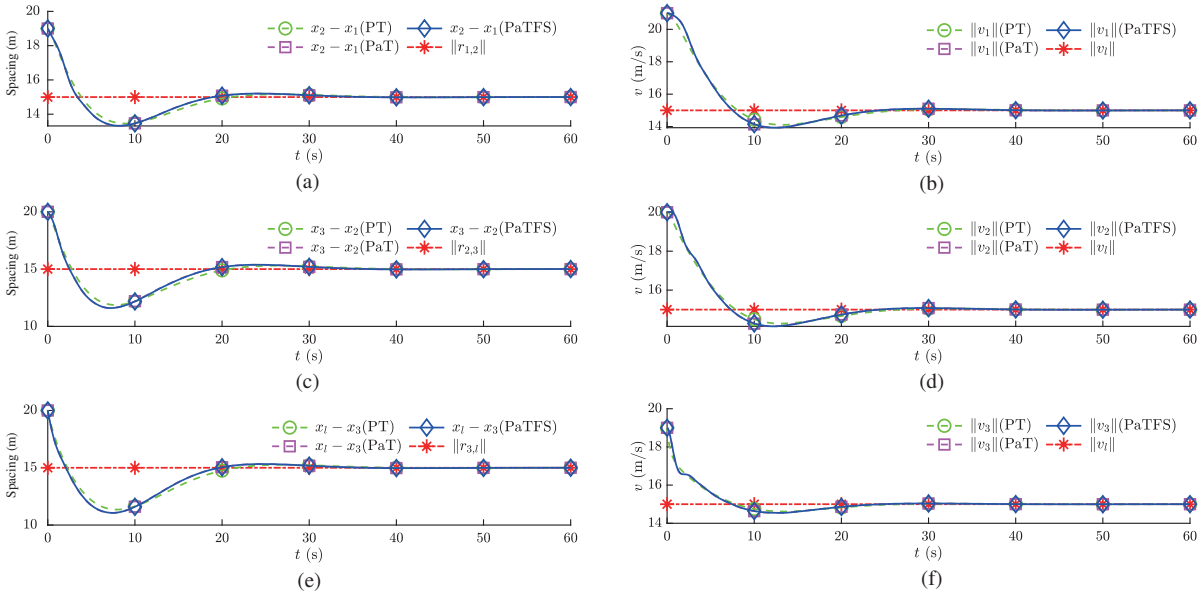

Figure 7 (Color online) The spacing evolution of PT, PaT, and PaTFS applied to each CAV is given in the left column. (a), (c) and (e) show the spacing between CAV 1, CAV 2 and CAV 3 and their predecessors. The reference spacing is given to demonstrate convergence. The velocities of PT, PaT and PaTFS applied to each CAV are given in the right column. (b), (d) and (f) show the velocities of CAV 1, CAV 2 and CAV 3. The reference velocity is given to demonstrate convergence.

distance and velocity fluctuations diminish, confirming the performance of PaTFS in achieving the theoretical desired platooning states. This is a direct conclusion from the results of P-PT and A-P.

The tracking performance was further evaluated through the root mean square (RMS) and final position errors of the three cases in Table 3. The A-P results show a precision of 10^{-4} m for the RMS and 10^{-7} m in the final value, proving excellent reference-following performance. The RMS values of the P-PT and A-PT models are in the order of 10^{-1} m depending on different CAVs, which reflects the trajectory differences between the PT and PaTFS. The final values of P-PT and A-PT reach 10^{-3} m in precision, demonstrating that the convergence to an accurate platoon configuration is achieved by the PT model.

5.1.2 *Spacing and velocities comparison*

The spacing and velocities depicted in Figure 7 highlight the longitudinal states of PaTFS, which comply with the PT model. The desired spacing between two adjacent CAVs is reached along with a final consensus in the velocity with respect to the leader's. The resemblance between the PaT and PaTFS performances arises from the same vehicle plant and similar longitudinal controls.

CAVs do not violate the minimum inter-vehicle distance constraints in any of the cases. PaT and PaTFS have almost identical performances, which is a direct reflection of the velocities depicted in Figures 7(b), (d), and (f). The responsiveness of the longitudinal control is desirable from a safety perspective. In the final platooning results, the PaT and PaTFS frameworks manage to reach spacing consensus precisely. It is safe to conclude that PaTFS is accurate and effective enough in longitudinal control.

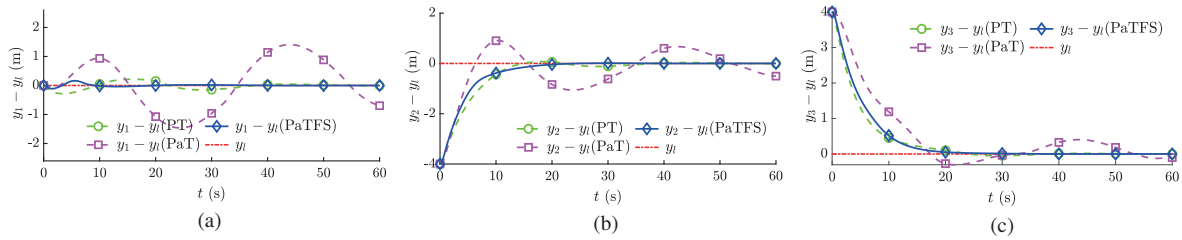

Figure 8 (Color online) The lateral deviations of CAV 1 (a), CAV 2 (b), and CAV 3 (c) from the desired lane respectively. The results of the cases where PT, PaT and PaTFS are applied to each CAV are all plotted. The desired lateral position is also plotted for each CAV as the reference.

Table 4 Lateral deviations of the CAVs from the desired positions under the PT, PaT and PaTFS models, respectively

	Scheme	CAV 1	CAV 2	CAV 3
RMS (m)	PT	0.1237	0.8667	0.8115
	PaT	0.8898	0.9556	1.1209
	PaTFS	0.03921	0.7994	0.8714
Final error (m)	PT	-7.0732×10^{-3}	-5.5593×10^{-3}	$-2.7976 \times 10-3$
	PaT	-0.6969	-0.5046	-0.1012
	PaTFS	4.9173×10^{-4}	3.7834×10^{-4}	1.9921×10^{-4}

5.1.3 *Lateral states comparison*

Figure 8 shows the varying lateral deviations of the different controllers. PT and PaTFS manage to shrink the multilane CAV configuration to a single-lane with trivial final deviations from the center of the desired lane. PaT, on the other hand, exhibits unfavorable overshoot and fluctuations for certain vehicles. In the merging process, compared with PaT, faster convergence with much fewer oscillations to the desired lane center is achieved through PaTFS, which is caused mainly by the feedforward steering term. The RMS values of lateral errors in Table 4 confirm this observation, with PaTFS having smaller RMS values for all CAVs compared with PaT.

Consistency with Figure 8 is also observed in the final values of the lateral errors in Table 4. All tracking errors of PT and PaTFS diminished. The RMS values of their lateral deviations are comparable, which conform to the fast merging actions of PaTFS. PaT, however, shows a degraded performance with larger RMS for all CAVs, which is a direct consequence of the obvious lateral sways along the lanes. The comparison demonstrates the superior performance of PaTFS in responsiveness and fine tracking accuracies compared to that of PaT. This result is further solidified with the final lateral deviations, in which PaTFS obtains precise position keeping while the fluctuations of the PaT fail to yield meaningful final deviations.

5.2 Scenario 2: distant and close case comparison with predefined trajectory tracking

A more complicated scenario was constructed to compare the PaTFS with a trajectory tracking controller demonstrating its vehicle-compatible actuation inputs and tracking performance.

Two cases were selected in this scenario: one with initially farther spaced CAVs and higher velocities, and another with tight spacing as well as lower velocities. We will refer to them as distant case and close case hereafter. In both cases, the following CAVs were expected to reach the desired same spacing and velocity settings as in scenario 1.

In this scenario, we include six following CAVs with the following consideration: for a random consecutive pair of CAVs, the combination of their roles, a predecessor or a follower, and their lane locations in the target lane or the adjacent lane, can find a corresponding pair among the six CAVs, which encloses the possible multilane initial conditions comprehensively. The parameters that are changed from the previous case are given in Table 5. Note that the CAVs 3 and 4 are merging CAVs initially located in adjacent lanes. The communication topology setting is still a bi-directional topology with nearest-neighbor communication. The corresponding adjacency matrix is a 6-by-6 matrix which is omitted here.

The adaptive cycloidal lateral trajectory (ACLT) in [29] for merging vehicles constrains the lateral acceleration perpendicular to the lane direction. It is chosen as a method for comparison because it features a representative methodology that depends on the predefined lane-changing trajectories to conduct

Table 5 Parameter settings for scenario 2

Symbol	Value		Unit
	Close case	Distant case	
$\boldsymbol{q}(0)$	$[0, 6, 15, 6, 30, 2, 45, 10, 60, 6, 75, 6]^{\mathrm{T}}$	$[10, 6, 30, 6, 50, 2, 65, 10, 80, 6, 100, 6]^{\mathrm{T}}$	m
$\boldsymbol{v}(0)$	$[17, 0, 17, 0, 18, 0, 18, 0, 16, 0, 16, 0]^{\mathrm{T}}$	$[20, 0, 20, 0, 21, 0, 21, 0, 19, 0, 19, 0]^{\mathrm{T}}$	m/s
$\boldsymbol{q}_l(0)$	$[90, 6]^{\mathrm{T}}$	$[120, 6]^{\mathrm{T}}$	m
r	$[-90, 0, -75, 0, -60, 0, -45, 0, -30, 0, -15, 0]^{\mathrm{T}}$		m
k	$[0, 0, 0, 0, 0, 1]$		–
γ	$\mathrm{diag}(8, 8)$		–

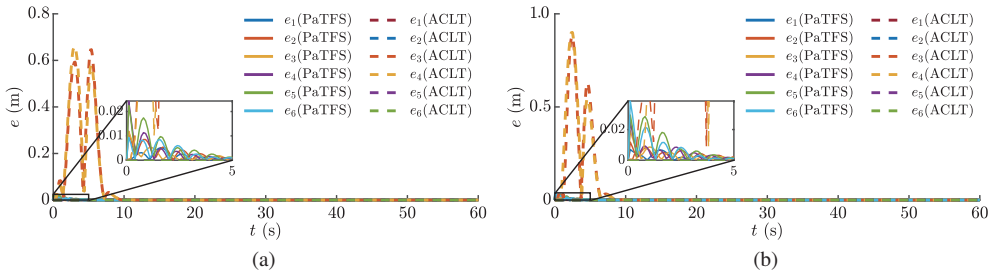

Figure 9 (Color online) The absolute tracking errors at each step for all CAVs in the (a) close and (b) distant cases, respectively. Absolute values are chosen for comparison. Note that ACLT only provides trajectories for the merging CAVs 3 and 4; the comparison of the tracking errors is thus based on these two CAVs. CAVs 3 and 4 exhibit larger deviations from the trajectories for ACLT. On the other hand, a much smaller magnitude of errors is observed when PaTFS is applied.

Table 6 Peak longitudinal and lateral acceleration of the CAVs

Scheme	Peak acceleration ($\mathrm{m/s^2}$)	Close case						Distant case					
		CAV 1	CAV 2	CAV 3	CAV 4	CAV 5	CAV 6	CAV 1	CAV 2	CAV 3	CAV 4	CAV 5	CAV 6
PaTFS	$\|a_x^{\mathrm{veh}}\|_{\max}$	0.728	1.014	1.348	2.138	1.943	1.055	1.279	1.182	1.996	2.141	3.560	3.646
	$\|a_y^{\mathrm{veh}}\|_{\max}$	0.112	0.734	3.085	1.945	1.182	0.280	0.128	0.693	2.664	1.632	0.978	0.204
ACLT	$\|a_x^{\mathrm{veh}}\|_{\max}$	7.248	4.491	3.584	4.203	3.729	1.773	22.500	16.406	10.896	8.448	11.667	6.463
	$\|a_y^{\mathrm{veh}}\|_{\max}$	0	0	3.169	3.007	0	0	0	0	3.305	2.741	0	0

merging control. As ACLT applies to the point model only, we replace the consensus control and reference generation parts of PaTFS framework with ACLT so that it can be applied to the vehicle plants. The maximum lateral acceleration is selected as $\|a_y\|_{\max} = 1\ \mathrm{m/s^2}$.

The merging and platooning task could be both fulfilled by the PaTFS and ACLT. On the other hand, the planning and tracking performance in Figure 9 illustrates their major differences. The PaTFS generates reference states at each step and the tracking errors descend to near zero values within approximately 10 s for all CAVs. The ACLT, though producing well-defined trajectories, generates errors in the order of 10^{-1} m in both the close and distant cases during the lane changing process, which are significantly larger. The settling time for all CAVs within 10 s is similar to that of PaTFS.

The peak acceleration values are listed in Table 6. In the close case, both ACLT and PaTFS exhibit reasonable acceleration inputs. In the distant case, different performances can be observed: for most CAVs, the ACLT implements higher peak accelerations, which may be impractical for real-vehicle actuation. The overly large accelerations in both longitudinal and lateral controls impede the tracking of the merging trajectory for CAVs 3 and 4, as the changing accelerations and velocities may hinder the precise steering during the tracking process. In this sense, a predefined trajectory would not always serve as an appropriate reference given the varying states of CAVs in different working conditions. In addition, the PaTFS in the distant and close cases produced comparable results, indicating their adaptiveness to different scenarios, as the tracking errors vanished in a similar fashion. The ACLT on the other hand, showed larger deviations from the planned trajectory during the merging operation in the distant case.

6 Conclusion and future work

This paper applies a newly designed controller consisting of multiagent coordination and a vehicle compatible control scheme to the context of multilane merging and platooning. Theoretical stability proof of the proposed distributed controller is given to guarantee that the desired platoon is asymptotically achieved with no inter-vehicle collisions. The PaTFS framework, which assembles the coordination scheme with controllers considering vehicle dynamics, is proposed and verified through a HiL experiment. Accuracy and responsiveness results were superior to those using conventional tracking methods. To enhance the comprehensiveness of the proposed control scheme, the formulation of higher fidelity models in the theoretical analysis along with practical limitations on vehicle states and control inputs will be considered in future work.

Acknowledgements This work was supported in part by National Key Research and Development Program of China (Grant No. 2017YFB0102503) and National Natural Science Foundation of China (Grant No. 52072243).

References

1 Li D Y, Liu M, Zhao F, et al. Challenges and countermeasures of interaction in autonomous vehicles. Sci China Inf Sci, 2019, 62: 050201
2 Hubmann C, Schulz J, Becker M, et al. Automated driving in uncertain environments: planning with interaction and uncertain maneuver prediction. IEEE Trans Intell Veh, 2018, 3: 5–17
3 Ntousakis I A, Nikolos I K, Papageorgiou M. Optimal vehicle trajectory planning in the context of cooperative merging on highways. Transport Res Part C-Emerging Technol, 2016, 71: 464–488
4 Baselt D, Knorr F, Scheuermann B, et al. Merging lanes—fairness through communication. Veh Commun, 2014, 1: 97–104
5 Liu H, Kan X D, Shladover S E, et al. Modeling impacts of cooperative adaptive cruise control on mixed traffic flow in multi-lane freeway facilities. Transport Res Part C-Emerging Technol, 2018, 95: 261–279
6 Zheng Z. Recent developments and research needs in modeling lane changing. Transport Res Part B-Meth, 2014, 60: 16–32
7 Kato S, Tsugawa S, Tokuda K, et al. Vehicle control algorithms for cooperative driving with automated vehicles and intervehicle communications. IEEE Trans Intell Transp Syst, 2002, 3: 155–161
8 Li S E, Zheng Y, Li K, et al. Dynamical modeling and distributed control of connected and automated vehicles: challenges and opportunities. IEEE Intell Transp Syst Mag, 2017, 9: 46–58
9 Englund C, Chen L, Ploeg J, et al. The grand cooperative driving challenge 2016: boosting the introduction of cooperative automated vehicles. IEEE Wireless Commun, 2016, 23: 146–152
10 Bengtsson H H, Chen L, Voronov A, et al. Interaction protocol for highway platoon merge. In: Proceedings of IEEE 18th International Conference on Intelligent Transportation Systems, Las Palmas, 2015. 1971–1976
11 Semsar-Kazerooni E, Elferink K, Ploeg J, et al. Multi-objective platoon maneuvering using artificial potential fields. IFAC-PapersOnLine, 2017, 50: 15006–15011
12 Goli M, Eskandarian A. A systematic multi-vehicle platooning and platoon merging: strategy, control, and trajectory generation. In: Proceedings of ASME 2014 Dynamic Systems and Control Conference, San Antonio, 2014. V002T25A006
13 You F, Zhang R, Lie G, et al. Trajectory planning and tracking control for autonomous lane change maneuver based on the cooperative vehicle infrastructure system. Expert Syst Appl, 2015, 42: 5932–5946
14 Zhou M, Qu X, Jin S. On the impact of cooperative autonomous vehicles in improving freeway merging: a modified intelligent driver model-based approach. IEEE Trans Intell Transp Syst, 2017, 18: 1422–1428
15 Plessen M G, Bernardini D, Esen H, et al. Spatial-based predictive control and geometric corridor planning for adaptive cruise control coupled with obstacle avoidance. IEEE Trans Contr Syst Technol, 2018, 26: 38–50
16 Li B, Zhang Y, Shao Z, et al. Simultaneous versus joint computing: a case study of multi-vehicle parking motion planning. J Comput Sci, 2017, 20: 30–40
17 Karagiannis G, Altintas O, Ekici E, et al. Vehicular networking: a survey and tutorial on requirements, architectures, challenges, standards and solutions. Commun Surv Tut, 2011, 13: 584–616
18 Liu J W, Huang J. Leader-following consensus of linear discrete-time multi-agent systems subject to jointly connected switching networks. Sci China Inf Sci, 2018, 61: 112208
19 Li Y, Li K, Zheng T, et al. Evaluating the performance of vehicular platoon control under different network topologies of initial states. Phys A-Stat Mech Its Appl, 2016, 450: 359–368
20 Calzolari D, Schürmann B, Althoff M. Comparison of trajectory tracking controllers for autonomous vehicles. In: Proceedings of IEEE 20th International Conference on Intelligent Transportation Systems, Yokohama, 2017. 1–8
21 Wang L, Wang X, Hu X. Connectivity maintenance and distributed tracking for double-integrator agents with bounded potential functions. Int J Robust Nonlin Control, 2015, 25: 542–558
22 Olfati-Saber R. Flocking for multi-agent dynamic systems: algorithms and theory. IEEE Trans Automat Contr, 2006, 51: 401–420
23 Zheng Y, Li S E, Wang J, et al. Stability and scalability of homogeneous vehicular platoon: study on the influence of information flow topologies. IEEE Trans Intell Transp Syst, 2016, 17: 14–26
24 Abe M. Vehicle Handling Dynamics: Theory and Application. Oxford: Butterworth-Heinemann, 2009
25 Su H, Chen M Z Q, Lam J, et al. Semi-global leader-following consensus of linear multi-agent systems with input saturation via low gain feedback. IEEE Trans Circ Syst I, 2013, 60: 1881–1889
26 Liao F, Teo R, Wang J L, et al. Distributed formation and reconfiguration control of VTOL UAVs. IEEE Trans Contr Syst Technol, 2017, 25: 270–277
27 Shladover S E, Nowakowski C, Lu X Y, et al. Cooperative adaptive cruise control: definitions and operating concepts. Transport Res Record, 2015, 2489: 145–152
28 Rodríguez-Seda E J, Stipanović D M, Spong M W. Guaranteed collision avoidance for autonomous systems with acceleration constraints and sensing uncertainties. J Optim Theor Appl, 2016, 168: 1014–1038
29 Goli M, Eskandarian A. Evaluation of lateral trajectories with different controllers for multi-vehicle merging in platoon. In: Proceedings of International Conference on Connected Vehicles and Expo (ICCVE), 2014. 673–678